Resolving the atomic structure of supported nanometer-size Au clusters

D. Lovall
Department of Physics, Purdue University, West Lafayette, Indiana 47907

M. Buss and R. P. Andres
School of Chemical Engineering, Purdue University, West Lafayette, Indiana 47907

R. Reifenberger
Department of Physics, Purdue University, West Lafayette, Indiana 47907

(Received 17 February 1998)

Field-ion microscopy (FIM) is used to resolve the atomic structure and orientation of individual nanometer-size Au clusters supported on sharp tips of W, Pt, and a Pt/Ir alloy. The FIM images from a single cluster illustrate that the technique is capable of providing atomically resolved images of supported nanometer-size clusters in an ultrahigh vacuum environment. By comparing computer simulations of a FIM image to experimental data, the atomic structure and orientation of the supported cluster can be determined. [S0163-1829(98)07528-6]

I. INTRODUCTION

Traditionally, the atomic structure of a small metal cluster has been investigated using high-resolution transmission electron microscopy (HRTEM) techniques. Interestingly, HRTEM images of nanometer-size metallic particles have provided evidence for structural fluctuations in the shape and orientation of supported clusters.[1–5] The origin of these structural fluctuations is of considerable interest since they may represent inherent limitations in the stability of any nanometer-scale structure fabricated from small numbers of metal atoms. New techniques to better investigate this issue would certainly be welcome.

In what follows, we discuss new results obtained by depositing nanometer-size Au clusters on the apex of sharp W, Pt, and Pt/Ir tips under UHV conditions. Having captured a Au nanocluster on a tip, we find it is possible using field-ion microscopy (FIM) techniques to image the corner and edge atoms on the nanocluster's upper surface. Using this approach important questions related to the structure, stability, diffusion, and orientation of the cluster can be addressed at the atomic level.

Previous studies of nanometer-size clusters deposited on the apex of sharp tips have been reported in the literature. Castro *et al.* first reported depositing and imaging nanometer-scale clusters on field emission tips to study the reduction in melting temperature of Au clusters as a function of cluster size.[6–8] Lin *et al.* subsequently reported features in the energy-resolved electron emission spectra from Au clusters[9–11] and C_{60} (Ref. 12) and attributed these features to the discrete electronic structure of the clusters.[9] Lin *et al.* also found indirect evidence for structural fluctuations by studying the stability of the electron current emitted from a supported cluster in the presence of a high electric field.[13] During the early stages of this work Castro, *et al.* succeeded in obtaining the first field-ion micrographs of a supported nanometer-size Au cluster.[6] We have since improved upon the experimental apparatus used by Castro *et al.* to allow a resolution of the cluster structure at the atomic level.

The atomic structure of a supported cluster is inferred by comparing experimental FIM images to simulated FIM images obtained by assuming different atomic structures and orientations for the cluster. We use a thin-shell model[14–16] to simulate FIM images from a cluster having an assumed atomic structure and compare these to the experimental images. With further refinements, this technique may offer an experimental method capable of confirming detailed predictions of cluster structure based on molecular dynamics (MD) calculations.[17,18]

II. EXPERIMENTAL CONSIDERATIONS

A. Cluster source

The Au clusters were prepared using a multiple expansion cluster source (MECS). A description of this cluster source can be found in the literature.[6,19,20] Briefly, it is a gas aggregation source designed to run with 20 to 50 torr of inert gas in the growth region. Cluster growth both via accretion of single atoms and via cluster-cluster aggregation can be promoted. A cluster beam is formed by expanding a small portion of the flow along the centerline of the condensation reactor into a vacuum chamber through a capillary nozzle. In the studies reported below, the clusters were annealed before being expanded into the vacuum chamber by passing through an annealing furnace.[21]

B. Cluster deceleration

MD calculations have shown that clusters deposited onto a substrate at high kinetic energies can suffer damage upon impact.[22–24] Cheng and Landman[22] considered Cu_{147} clusters incident on a (111)-oriented Cu surface. They found that significant damage (cluster deformation and mixing of surface and cluster atoms) occurred for impacts where the kinetic energy was greater than ~ 1 eV/atom, or for cluster speeds of greater than 2 km/s. Betz and Husinsky studied Al

and Pb clusters impinging on Cu surfaces, with similar results.[23] Minimal damage occurred for collisions with an average kinetic energy of <1 eV/atom.

In the Purdue MECS, the clusters are swept along in a He carrier gas. After passing through the annealing furnace, the cluster/gas mixture passes into a vacuum chamber through a 1-mm-diameter capillary tube. The flow through this tube determines the impact velocity of the clusters on substrates. There are two cases worth considering.

In case 1, the velocity of the cluster is completely established by the flow inside the capillary tube. In this case, we make the assumption that the cluster speed is equal to that of the carrier gas at the exit of the capillary. This sets a lower limit for the cluster speed. The appropriate velocity under these circumstances is given by[25]

$$v_{p,\mathrm{lower}}=\frac{1}{2}\sqrt{\frac{\gamma kT_c}{m_g}} \tag{1}$$

with $\gamma=1.67$ being the specific heat ratio of the He carrier gas. T_c and m_g are respectively the temperature of the capillary and mass of the carrier gas, while k is Boltzmann's constant. For He, this implies a cluster speed of about 510 m/s, or a kinetic energy of ~ 0.26 eV/atom for Au clusters.

In case 2, the velocity of the cluster is determined by the free jet expansion of the He upon exiting from the capillary tube and entering the main vacuum chamber. Clusters will be accelerated in this expansion via collisions with gas molecules. Depending on the number of collisions, the cluster speed could become equal to the final mean speed of the gas molecules. This sets the upper limit for the cluster speed given by[25]

$$v_{p,\mathrm{upper}}=\sqrt{\frac{5kT_c}{m_g}}. \tag{2}$$

If we assume complete acceleration, the clusters based on this scenario could attain a velocity of ~ 1770 m/s, corresponding to an energy of ~ 3.2 eV/atom for Au clusters.

Both of these cases indicate that the cluster can acquire sufficient energy to inflict significant damage upon impacting the tip. The clusters must therefore be decelerated prior to deposition.

The clusters are decelerated by passing them through a box, which is held at a higher pressure than the MECS vacuum chamber by leaking in Ar gas. The distance $X_{\max}$ required to stop a particle with diameter d_p, density ρ_p, and velocity v_p traveling through a stagnant gas at a temperature T_g and with a number density n_g is[26]

$$X_{\max}=\left(\frac{2}{8+\pi}\right)\frac{d_p\rho_p v_p}{n_g m_g}\left(\frac{\pi m_g}{2kT_g}\right)^{1/2}. \tag{3}$$

This equation assumes that the decelerating gas molecules have a Boltzmann distribution of thermal velocities. $X_{\max}$ is found experimentally by monitoring the cluster flux with a film thickness monitor (FTM) and adjusting the pressure in the deceleration cell until the FTM signal drops to 50% of the FTM signal prior to deceleration. When this occurs, $X_{\max}$ is roughly equal to the length of the deceleration cell, ~ 61 cm in the current configuration. Clusters that pass through the cell are then assumed to have a thermal velocity distribution set by T_g, the temperature of the gas in the deceleration box.

As can be seen from Eq. (3), smaller clusters are decelerated more than larger clusters while the smallest clusters tend to be stopped completely. This prediction can be checked by monitoring the size distribution of the cluster beam before and after deceleration. If an initial size distribution of clusters passes through the deceleration box, the smaller clusters will be filtered out, while larger clusters will pass through. This filtering will result in a change in the size distribution. This was studied by sampling the cluster beam both before and after the deceleration box. As in previous studies,[7,8,13,27,10,11] samples of the clusters in the beam are captured on amorphous carbon grids for analysis by TEM.[19,20] Analysis of TEM micrographs taken in conjunction with the present experiments allowed a measure of the cluster size distribution before and after deceleration. The results of these studies confirm that because of the narrow size distribution produced by the MECS there is little change in the mean cluster diameter on deceleration and suggest that the initial velocity of clusters *before* they enter the deceleration box is between the values predicted by Eqs. (1) and (2). This is reasonable, since it is likely that there are insufficient collisions to accelerate the clusters to the maximum velocity given by Eq. (2).

Clusters having a mass m_c and exiting from the deceleration box have a final mean thermal velocity given by

$$v_{p,f}=\sqrt{\frac{8kT_g}{\pi m_c}}. \tag{4}$$

For a 2 nm diameter spherical Au cluster, $v_{p,f}=4.0$ m/s, corresponding to an impact kinetic energy of 1.6×10^{-5} eV/atom. This velocity is sufficiently small to assure a soft landing.

C. FEM/FIM chamber

The FIM is housed inside a UHV chamber pumped by a 220 l/s ion pump. During FIM imaging, the chamber can be isolated from the ion pump by means of an 8-in. gate valve.

In order to capture clusters on FIM tips, the tip must be placed in a cluster beam approximately 2 mm in diameter. To do this reliably, tips are mounted on a sample manipulator that has three degrees of translational and two degrees of rotational freedom. The sample mounting stage also has three degrees of translational freedom and two degrees of rotational freedom, enabling us to precisely align the tip with the cluster beam. The sample holder on the XYZ-R manipulator was further modified to allow use of the high voltages necessary in the FIM. A 5-mm-thick macor block was added to the top of the stage for high voltage insulation.

Tips are mounted on modified electron gun filament holders. The filaments have been replaced with a W support loop to which the tips (i.e., substrates) are spot welded. The filament holder plugs into two stainless steel sockets on the mounting stage, which greatly simplifies tip replacement. A Cu collar attached to the manipulator's LN_2 reservoir fits around the ceramic base of the tip holder so that the tip can be cooled to near 100 K as calibrated by a nearby thermocouple.

The cluster beam passes into the UHV chamber via a 2.75-in. port, after passing through a 4-way cross that is differentially pumped with a turbo pump. A Cu septum with a 3.18-mm-diam capillary tube that is 50 mm long separates the UHV FIM from the differentially pumped space, which is located down line from the deceleration cell. This arrangement protects the UHV chamber from contaminants present in the main vacuum chamber, keeping the pressure in the FIM around 10^{-9} Torr during cluster deposition. During FIM operation, a gate valve is used to separate the two chambers.

D. Cluster capture

During cluster capture, the cluster beam passes through a small probe hole in the fluorescent screen. The tip is aligned with the cluster beam and pointed at the screen so that the progress of cluster capture can be monitored. Individual Au clusters were deposited on suitably etched Pt or W tips mounted on a support loop and carefully aligned with the 2 mm diameter cluster beam using a theodolite. The tip is pointed toward a fluorescent screen and biased to promote field emission of electrons. Before deposition, the characteristic field emission pattern from the tip is observed at some voltage V_0, which is typically about 2000 V. The arrival of an individual cluster can be detected by relying on the well-known fact that field emission current density J is given by

$$J = AF^2 e^{-B/F}, \tag{5}$$

where F is the local electric field and A and B are constants. The local electric field F can be related to the applied voltage V using

$$F = \frac{V}{kR} = \beta V, \tag{6}$$

where R is the local radius of curvature and k is a constant related to the emitter geometry. For a standard field emission tip k is typically ~ 5, but this can be quite different for the geometry used here.

The procedure we have developed to detect a cluster arrival is to lower the voltage on the tip to $\sim \frac{2}{3} V_0$, causing the field emission pattern from the tip to disappear. The deposited nanocluster has a small radius of curvature, which results in a strong localized electron emission and the appearance of a bright spot on the screen.

The mean time to capture a cluster on the tip can be crudely estimated from

$$\Delta t = (\pi R^2 \mathcal{F})^{-1}, \tag{7}$$

where R is the tip radius and $\mathcal{F}$ is the cluster flux. A cluster flux in the undeccelerated beam of about 1×10^{10} clusters/cm^2 s is typical. Assuming perfect alignment of the cluster beam with a tip of typical radius 100 nm, and the cluster flux quoted above, the mean time of arrival between clusters is estimated to be ~ 3 s. This is in reasonable agreement with the 5–10 s usually required to capture a cluster on the tip if no deceleration is used. In circumstances where clusters are decelerated prior to deposition, the cluster beam is significantly diffused and the capture time increases to ~ 5–10 min.

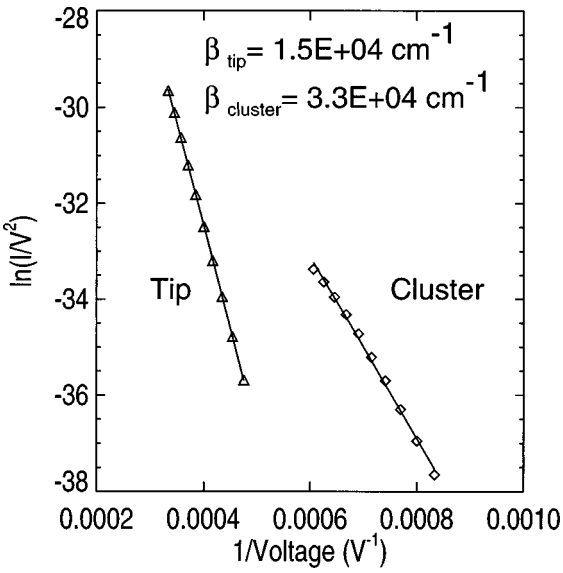

FIG. 1. Fowler Nordheim data illustrating the electron emission characteristics of a clean W tip and a cluster captured on the tip. The approximate value for the proportionality constant β relating the electric field to the applied voltage is also given.

As soon as localized electron emission is observed at a reduced voltage, the voltage is further reduced to about $\frac{1}{2} V_0$ and the cluster beam is blocked off by closing a gate valve. The electron emission characteristics of the cluster can be measured by studying the current as a function of the applied voltage and using Eq. (5). A representative Fowler-Nordheim plot is shown in Fig. 1 and illustrates how the electron emission characteristics change after the cluster is soft landed on a tip.

E. Cluster imaging

Electron emission from the cluster can be imaged by rotating the tip toward a multichannel plate equipped with an integral phosphor screen. A video camera and VCR are used to record the emission pattern for further analysis, providing a time resolution of 1/30 s. A frame grabber and PC allow individual frames to be captured and analyzed in more detail. If the cluster location on the tip is not deemed suitable, the cluster can be removed by pulsing the tip support loop with sufficient current to thermally desorb the cluster. The cluster capture procedure can then be quickly repeated until a more suitable cluster is obtained.

Before imaging in the FIM mode, $\sim 2 \times 10^{-5}$ Torr of Ar imaging gas is admitted into the UHV chamber and the polarity of the voltage applied to the tip is reversed. The tip/cluster is cooled using a liquid nitrogen cold finger to a temperature of about 100 K. Ar was chosen as an imaging gas based upon its relatively low best image field (BIF).[16] Upon raising the voltage to $\sim 3 V_0$, inspection of the *same* region of the phosphor screen used to observe field emission from the cluster reveals an unmistakable pattern of field-ion spots. The intensity of these spots depends exponentially on the local electric field. Since the field is expected to vary in a complicated way around the nanometer-size cluster, it is not too surprising that the image spots produced by different

atoms on the cluster vary greatly in brightness. Since FIM is essentially a point projection technique, the overall magnification is given by

$$M = \frac{R}{\rho r}, \tag{8}$$

where R is the tip to screen distance, r is the cluster radius, and ρ is a field compression factor that is expected to be close to unity. For the system described here, M can be as large as $\sim 100 \times 10^6$.

III. COMPUTER SIMULATION OF FIELD-ION MICROSCOPY IMAGES

The thin shell model[14–16] was adopted for computer simulations of the FIM images of the clusters. This model assumes that field-ion images are formed on a screen by the outermost atoms on the surface of the cluster where the local electric field is the largest. This approach has been used extensively for simulating images of unknown crystal structure. In our implementation of this technique, a cluster structure must first be assumed. For completeness in our simulations, both icosahedral (13 atoms, 55 atoms, 147 atoms, etc.) and truncated octahedral (38 atoms, 201 atoms, 586 atoms, etc.) structures were considered. The clusters captured almost certainly have additional adatoms on the outer facets, most of which are field desorbed during the initial imaging process. The cluster that remains is assumed to be reasonably well approximated by the ''magic'' number clusters containing closed shells of atoms used in our simulations.

We apply the thin shell criterion to determine which atoms in the cluster contribute to the field-ion image. If an atom is identified as potentially contributing to the final image, its position, for a specified rotation of the cluster, is computed. If the atom falls in the hemisphere facing the screen, the image of that atom is projected to simulate the trajectories of imaging Ar gas ions in the field-ion microscope. A schematic of this implementation is shown in Fig. 2. This method has been applied to feasibility studies related to resolving cluster structure elsewhere.[28] The shell thickness t was treated as a convenient parameter to discriminate exactly which atoms on a cluster are imaged. After the best orientation of the cluster was determined, the shell thickness was further adjusted to provide the best fit to the experimental data.

In our implementation, the simulated FIM image is formed by a simple geometric projection of the atoms contributing to the image. The point of projection is assumed to be a distance nR from the front surface of the cluster where R is the radius of the cluster. When $n=2$, a stereographic projection results. Prior studies have indicated this is closest to actual results,[29] and gives a good approximation of the expected images.

The coordinates for the atoms in the clusters used in our simulations were generated using a molecular dynamics simulation program and represent the relaxed equilibrium structure at 0 K.[24] A computer program was written to allow a rotation of each cluster through any combination of standard Euler angles θ, ϕ, and ψ.[30] On some occasions, additional atoms were added or subtracted to the surface facets to optimize the fits to the experimental FIM images.

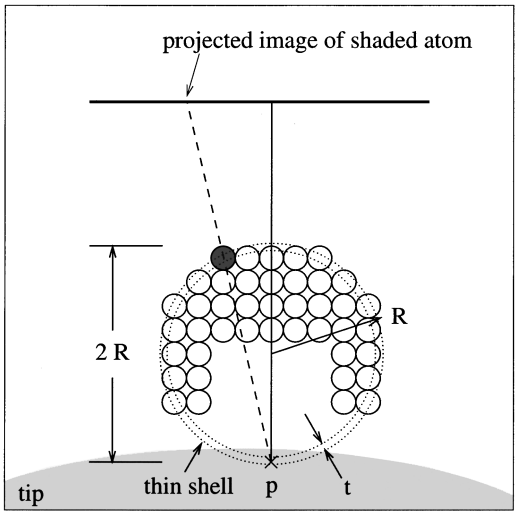

FIG. 2. Schematic of the thin shell model used in this study for simulating field ion micrographs of supported nanometer-size cluster of radius R. Any atom whose center falls within the thin shell is considered to contribute to the final image. The image projection point P is located a distance $2R$ behind the front surface of the cluster.

IV. RESULTS

Our initial studies have shown that after proper alignment of the tip, it is always possible to capture a cluster within a few minutes after exposing the tip to the cluster beam. The initial FIM images of a captured cluster are sometimes found to be uneven and, occasionally, the entire cluster will desorb during the initial imaging procedure. The uneven nature of the image is thought to be due to field desorption of weakly bound Au atoms from the cluster facets. After a few minutes, however, a stable image of the cluster usually becomes evident. Of the clusters captured, approximately 50% survive to produce field-ion images. Using this technique, it has been possible to image the atomic structure of clusters that have been prepared in a variety of different ways and landed on tips of different composition.

A. Characteristics of the initial FIM images

The initial FIM imaging of Au clusters tended to be very unstable and difficult to interpret. Image spots of corner or edge atoms on the cluster were sparse, with only one or two initially appearing. Composite mapping was attempted to better understand this result. As an example, a composite FIM map was constructed by superimposing 15 images taken over a time span of about 5 min. The composite map [see Fig. 3(a)] reveals regions in which no atoms are imaged, whereas other regions yield many imaged atoms. Examination of such maps shows that the regions imaged tend to lie along lines that outline facets of the cluster, as suggested by the construction shown in Fig. 3(b). This interpretation suggests a process in which weakly bound Au atoms migrate across the cluster, become stuck at a cluster edge, and then field evaporate.

This interpretation is supported by subsequent FIM images obtained from the cluster. Some clusters showed a remarkable degree of stability, even though not enough edge

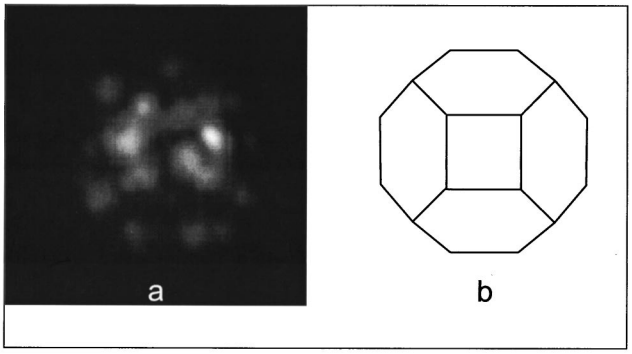

FIG. 3. (a) Composite field-ion images of an annealed cluster deposited on a W tip, showing the underlying structure represented in (b). This image was formed by combining 15 images captured from a 5-min section of the videotape. The imaging gas was Ar and the tip was held at 100 K.

and corner atoms were imaged to allow an unambiguous structural determination. Other clusters exhibited images of enough atoms to warrant extensive analysis. Examples of such images are shown in Figs. 4 and 6 below. Each of these images followed periods of image instability as discussed above. These FIM images were quite stable for periods between ~ 30 sec and ~ 15 min before deteriorating as the applied voltage was adjusted in an effort to obtain the best imaging conditions.

Taken together, these observations suggest the presence of an underlying core structure with ''extra'' atoms on the surface that are initally imaged. Because of the large local enhancement of the electric field around these ''extra'' atoms, they tend to migrate toward regions of high electric field. The underlying core structure is not initially imaged until the surface atoms are removed via field desorption.

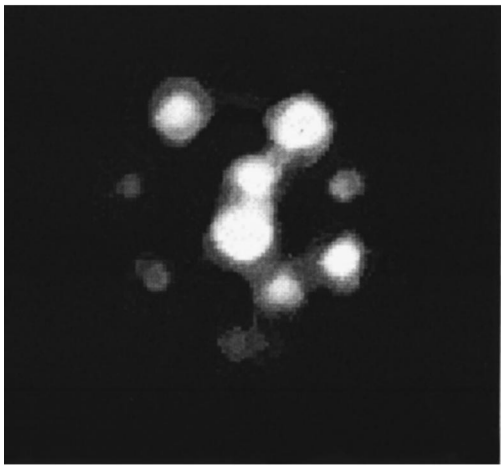

FIG. 4. A field-ion image from a ~ 1.5 nm Au cluster, annealed before deposition at a temperature of 1200 K, cooled to 300 K, and landed on a W tip. The imaging gas is Ar and the temperature of the tip and cluster is 100 K.

B. Annealed Au cluster on a W tip

Clusters captured on W tips were often observed to wet the surface shortly after landing. Instances of cluster wetting were found to be distinct and readily identifiable. As previously mentioned, the arrival of a cluster on the tip is signified by the appearance of a bright spot on the phosphor screen. In cases where the cluster wets the tip, this bright spot would dim at a given voltage, and would often increase in apparent size. We interpreted this as being caused by a decrease in the local electric field surrounding the cluster, implying that the cluster had spread out over the surface of the tip. For W tips, if the tip were very clean at the time of capture, wetting would sometimes take ~ 10 s. For dirtier W tips, Pt tips, and Pt/Ir tips, wetting would often take several minutes. In some extreme cases, wetting would take place over the course of several hours. During this time, the voltage required to image the cluster would increase steadily, implying that the radius of the cluster was steadily increasing.

The wetting rate is thought to be related to the surface condition of the W tip. Qualitatively, clusters that were captured shortly after pulse cleaning of the tip were more likely to wet the surface than clusters captured several minutes afterward. Similarly, the wetting rate decreased as the time after pulse cleaning increased. This indicates that the interaction force between a clean W surface and a nanometer-size Au cluster is strong. As the surface becomes covered with residual background gas, the interaction becomes weaker.

In some cases, FIM imaging was performed *after* cluster wetting was observed in the field emission mode. Images of Au cluster atoms were identifiable at the expected location up to electric fields of ~ 260 MV/cm. Even in cases where the entire cluster was field desorbed during the initial stages of FIM imaging, a return to field emission mode would reveal areas of enhanced electron emission at the location where the cluster had been.

Interestingly, the clusters seemed to preferentially avoid certain areas of the tip. Clusters were seldom seen to stick to W(110) facets, and were usually located on the rougher, less densely packed regions instead. Whether the clusters actually did not land on the W(110) facets or quickly migrated from them is unknown. The few clusters that did land on W(110) were observed to wet this surface.

These observations are reminiscent of studies of Au migration on W by other authors.[31–33] Jones observed that Au atoms evaporated onto a W tip were repelled from the most densely packed planes [like the W(110) facet] having the highest surface free energy. This behavior continued until a critical coverage was reached, and the Au subsequently ''invaded'' the W(110) regions.

A FIM image of an Au cluster deposited on a W tip is shown in Fig. 4. The white spots in the images represent individual atoms protruding from the exposed surface of the Au cluster. Clear evidence for a hexagonal facet is provided by even a quick examination of these images. The rate of ionization (and hence the intensity recorded on the microchannel plate) depends exponentially on the local electric field.[34] Thus, the observed variation in brightness between the images of the individual atoms is attributed to small local differences in the electric field around the three-dimensional cluster. The hexagonal symmetry apparent in the image

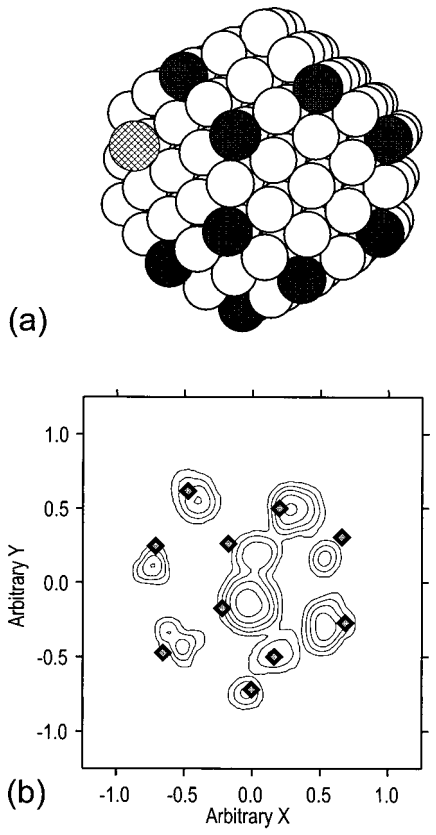

FIG. 5. (a) A 202-atom cluster shown in the orientation that best fits the experimental image in Fig. 4. The darkened atoms represent the atoms imaged in the experiment. The atom shaded with a cross-hatched pattern represents an atom added onto a surface facet to improve the fit to the experimental image. (b) Comparison of a simulated FIM image of a 202-atom cluster to the experimental image in Fig. 4.

identifies this cluster as a member of the TO family. Comparisons to simulated images identify this cluster as being based on a 201-atom core, with a few extra atoms on the surface facets.

A comparison between the experimental image and the best simulation is shown in Fig. 5. The resulting comparison between the simulated FIM image (squares) and the experimental image (represented as an intensity contour plot) is given in 5(b). The two show good agreement. The hexagonal face on the right side of the image appears to be more compressed in the X direction in the experimental image than in the simulated image; this might be explained by the position of the cluster on the tip. In this case, the cluster landed far from the apex of the tip, resulting in a distortion of the electric field lines. The simulations do not account for this and so are not capable of reproducing this effect.

C. Annealed Au cluster on a Pt tip

Pt tips were used in an effort to more fully understand the interactions between the tip and the Au clusters. Pt has been more widely used than W as a tip material in studying single-atom diffusion of Au atoms.[35]

Cluster capture was performed in a manner identical to that used with W tips, with similar success. Au clusters deposited on Pt tips did not exhibit the tendency to wet the tip as readily as those deposited on W tips. Electron emission from the cluster, conducted over a period of a few days, showed little evidence of either cluster diffusion or wetting of the Pt tip.

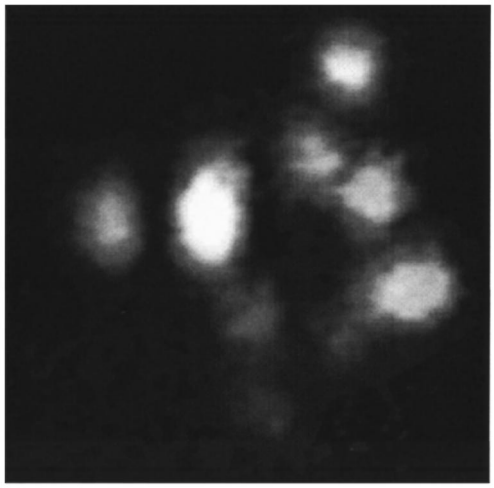

FIG. 6. A field-ion image from a ~ 1 nm Au cluster, annealed before deposition at a temperature of 1200 K, cooled to 300 K, and soft landed on a Pt field emission tip. The approximate temperature of the tip and cluster is 100 K. This image was formed by integrating two frames captured from the video tape.

An example of the field-ion image from a Au cluster on a Pt tip is shown in Fig. 6. A systematic examination of simulated FIM images quickly revealed that the cluster imaged in Fig. 6 is based on a 38-atom TO structure. The best orientation of the 38-atom cluster that agrees with experiment is shown in Fig. 7(a). The resulting comparison between the simulated FIM image (squares) and the experimental image (represented as an intensity contour plot) is given in 7(b). To optimize the agreement, an additional atom was added to the 38-atom core cluster. The atoms contributing to the final image are all found to be corner atoms and are shaded in Fig. 7(a). From this fit, we infer that a flat hexagonal cluster facet must be resting on the tip.

From Fig. 7(b), there is a small discrepancy between the projected atomic position and that measured experimentally, especially for those atoms located along the outermost perimeter of the cluster structure. At the present time, we believe this discrepancy can be attributed to the complicated local electric fields that influence the ion's trajectory immediately after ionization occurs. Choice of the projection point used in the simulations may have also been a factor, since a true stereoscopic projection was assumed for the simulated images.

D. Unannealed Au clusters on a Pt/Ir tip

Unannealed Au clusters were also studied. These clusters were deposited on Pt/Ir tips. The Pt/Ir tips were found to be much more robust than tips made from pure Pt. While they will not withstand the high temperatures normally used to pulse clean W tips, they can be repeatedly pulse cleaned at lower temperatures. Like Pt, and in contrast to W, the orientation of the Pt/Ir tip is unpredictable. Some tips were (111) oriented while the majority were (100) oriented.

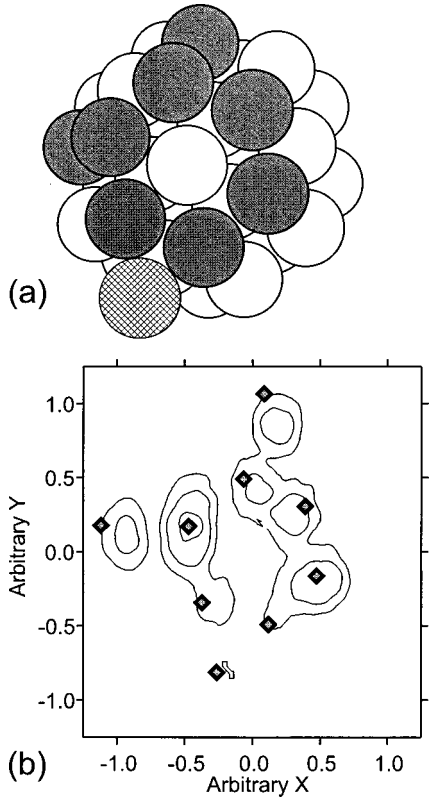

FIG. 7. (a) The 39-atom cluster shown in the orientation that best fits the experimental FIM image shown in Fig. 6. The darkened atoms represent those atoms imaged in the experiment. The atom shaded with a cross-hatched pattern represents an atom added onto a surface facet to improve the fit to the experimental image. (b) The simulated FIM micrograph (squares) of the 39-atom TO Au cluster shown in (a). The contour plot shows the intensity profile of the recorded FIM image from Fig. 6.

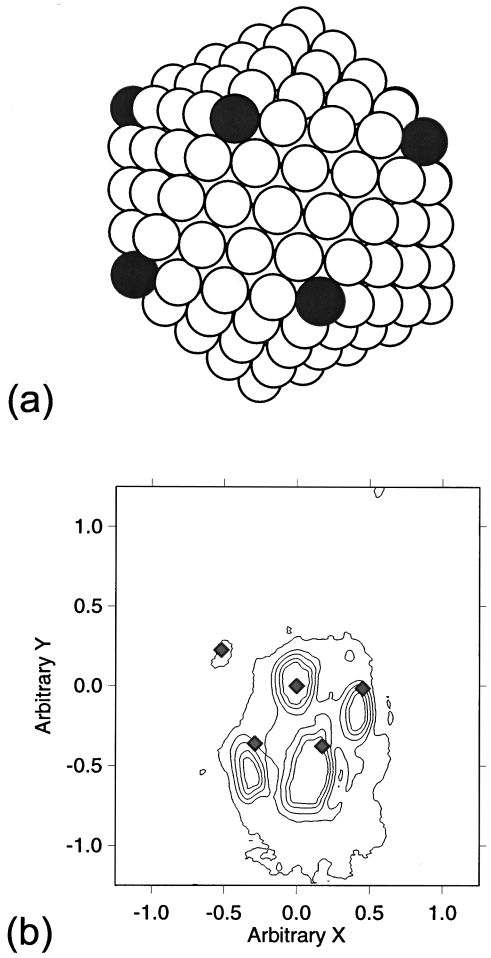

FIG. 8. (a) Proposed icosahedral structure required to explain the FIM image of an unannealed Au cluster on a Pt/Ir tip. The shaded atoms are those which contribute to the FIM image. (b) A comparison of the simulated image (squares) from the structure in (a) to the experimental image (intensity contours). The two show fair agreement. Discrepancies suggest that the cluster is either deformed by the substrate or derived from a structure other than a ''perfect'' icosahedron.

Previous FIM studies by Castro[36,6] have shown that unannealed Au clusters are expected to be multiply twinned particles. As shown previously,[28] simulations of FIM images from icosahedral clusters when compared to simulated images from truncated octahedral clusters are expected to show significant differences.

An example of a contour plot made from the recorded FIM image of an unannealed Au cluster deposited on a Pt/Ir tip is shown in Fig. 8(b). This cluster landed near one of the off-apex (100) facets of the tip. It was possible to image this cluster at 4.8 kV, considerably lower than the best image voltage of $\sim$10.5 kV for the bare tip. As the voltage was slowly increased, the dominant four atoms imaged dramatically increased in brightness and their image spots became badly smeared. This suggests that they lie on corners of the cluster, since the electric field there would have a high local enhancement. Close inspection of Fig. 8(b) reveals the positions of a few additional atoms, which became barely visible when imaged at higher fields. The positions of these atoms are best resolved using a contour plot of the intensity recorded from the FIM images.

It was impossible to obtain a good fit to the FIM image of the unannealed Au cluster using a structure from the TO family and therefore an icosahedral structure was used with slightly more success. Comparison of the FIM image to an icosahedral simulation did provide a match as shown by the location of the solid squares in Fig. 8(b). The atomic structure corresponding to this is shown in Fig. 8(a).

V. CONCLUSIONS

The use of field-ion microscopy (FIM) in conjunction with techniques for simulating field-ion images shows promise as a method for studying the atomic structure of supported metal clusters in the nanometer-size range. This technique seems to be one of the few that are capable of imposing an experimental constraint on the detailed predictions commonly obtained from molecular dynamic simulations of cluster structure for very small clusters.

The utility of this technique has been illustrated by comparing experimental FIM images of soft landed, annealed, and unannealed Au clusters with simulated FIM images of closed shell truncated octahedral and icosahedral nanocrystals of Au. Identification of one cluster as a 39-atom Au cluster and another cluster as a 202-atom Au cluster, both

having a truncated-octahedra structure, has resulted. The structure of an unannealed Au cluster could not be fit using a truncated-octahedra structure.

While we have observed clusters that we have tentatively identified as TO+ clusters, none of the so-called Marks decahedra (M-Dh) clusters[5] has been identified in the current study even though free space, MD calculations suggest they have the lowest total energy in the size range studied.[18]

ACKNOWLEDGMENTS

This work was partially funded by the National Science Foundation under Contract No. 9522248-CTS. The authors would like to thank Dr. D. Paithankar for providing the coordinates of atoms in the clusters used for the simulations, and Dr. T. Castro and Dr. G. Kellogg for helpful discussions during the initial phase of this work.

[1] S. Iijima and T. Ichihashi, Phys. Rev. Lett. **56**, 616 (1986).
[2] P. M. Ajayan and L. D. Marks, Phys. Rev. Lett. **60**, 585 (1988).
[3] J. Dundurs, L. D. Marks, and P. M. Ajayan, Philos. Mag. A **57**, 605 (1988).
[4] D. Narayanaswamy and L. D. Marks, Z. Phys. D **26**, S70 (1993).
[5] L. D. Marks, Rep. Prog. Phys. **57**, 603 (1994).
[6] T. Castro, Y. Z. Li, R. Reifenberger, E. Choi, S. B. Park, and R. P. Andres, J. Vac. Sci. Technol. A **7**, 2845 (1989).
[7] T. Castro, R. Reifenberger, E. Choi, and R. P. Andres, Surf. Sci. **234**, 43 (1990).
[8] T. Castro, R. Reifenberger, E. Choi, and R. P. Andres, Phys. Rev. B **42**, 8548 (1990).
[9] M. E. Lin, R. P. Andres, and R. Reifenberger, Phys. Rev. Lett. **67**, 477 (1991).
[10] M. E. Lin, R. Reifenberger, and R. P. Andres, Phys. Rev. B **46**, 15 490 (1992).
[11] M. E. Lin, R. Reifenberger, A. Ramachandra, and R. P. Andres, Phys. Rev. B **46**, 15 948 (1992).
[12] M. E. Lin, R. P. Andres, R. Reifenberger, and D. R. Huffman, Phys. Rev. B **47**, 7546 (1993).
[13] M. E. Lin, A. Ramachandra, R. P. Andres, and R. Reifenberger, in *Nanosources and Manipulation of Atoms under High Fields and Temperatures: Applications*, edited by Vu Thein Binh, N. Garcia, and K. Dransfeld, (Kluwer Academic, Boston, 1993), pp. 77–88.
[14] A. J. W. Moore, J. Phys. Chem. Solids **23**, 907 (1962).
[15] E. W. Müller and T. T. Tsong, *Field Ion Microscopy, Principles and Applications* (American Elsevier, New York, 1969).
[16] M. K. Miller and G. D. W. Smith, *Atom Probe Microanalysis* (Materials Research Society, Pittsburgh, PA, 1989).
[17] C. L. Cleveland, U. Landman, M. N. Shafigullin, P. W. Stephens, and R. L. Whetten, Z. Phys. D **40**, 503 (1997).
[18] C. L. Cleveland, U. Landman, T. G. Schaaff, M. N. Shafigullin, P. W. Stephens, and R. L. Whetten, Phys. Rev. Lett. **79**, 1813 (1997).
[19] Seung Bin Park, Ph.D. thesis, Purdue University, 1988.
[20] E. Choi and R. P Andres, in *Physics and Chemistry of Small Clusters*, edited by P. Jena, B. K. Rao, and S. N. Khanna (Plenum Press, New York, 1987), p. 61.
[21] A. N. Patil, D. Y. Paithankar, N. Otsuka, and R. P. Andres, Z. Phys. D **26**, 135 (1993).
[22] H.-P. Cheng and U. Landman, Science **260**, 1304 (1993).
[23] G. Betz and W. Husinsky, Nucl. Instrum. Methods Phys. Res. B **122**, 311 (1997).
[24] Dilip Paithankar, Ph.D. thesis, Purdue University, 1994.
[25] Seung Bin Park, Ph.D. thesis, Purdue University, 1988.
[26] T. K. Nguyen and R. P. Andres, Prog. Astronaut. Aeronaut. **74**, 627 (1981).
[27] T. Castro, E. Choi, Y. Z. Li, R. P. Andres, and R. Reifenberger, in *Clusters and Cluster-Assembled Materials*, edited by R. S. Averback *et al.*, MRS Symposia Proceedings No. 206 (Materials Research Society, Pittsburgh, 1991), p. 159.
[28] D. Lovall, R. P. Andres, and R. Reifenberger, in *Science and Technology of Atomically Engineered Materials*, edited by P. Jena, S. N. Khanna, and B. K. Rao (World Scientific, Singapore, 1996), pp. 137–146.
[29] R. Smith and J. M. Walls, J. Phys. D **11**, 409 (1978).
[30] Herbert Goldstein, *Classical Mechanics* (Addison-Wesley, New York, 1980).
[31] E. W. Plummer and T. N. Rhodin, J. Chem. Phys. **49**, 3479 (1968).
[32] A. Cetronio, Surf. Sci. **44**, 109 (1974).
[33] J. P. Jones, J. Solid State Chem. **104**, 149 (1993).
[34] T. T. Tsong, *Atom Probe Field Ion Microscopy* (Cambridge University Press, New York, 1990).
[35] G. L. Kellogg, Surf. Sci. Rep. **21**, 1 (1994).
[36] Tom Castro, Ph.D. thesis, Purdue University, 1989.